Active Rectification for the Optimal Command of Bidirectional Resonant Wireless Power Transfer Robust to Severe Circuit Parameters Deviations

Alexis Desmoort, *Student Member, IEEE,* Olivier Deblecker, *Member, IEEE,* and Zacharie De Grève, *Member, IEEE*

***Abstract*—In this paper, a method resorting to active rectification for the optimal control of a bidirectionnal resonant wireless power transfer system is proposed. Benefiting from a dual active bridge topology and without requiring any additional DC-DC converter, the real and the imaginary parts of the equivalent load impedance are modulated simultaneously and independently, for achieving optimal operating conditions despite circuit parameters deviations. Based on a first harmonic analysis, the methodology and its beneficial impacts against variations in the windings mutual inductance or against mistuned resonant capacitor are presented and illustrated. By an argued discussion, the proposed method extent is enlarged to changes in any circuit parameters. Time-domain simulations of the converters topology and command demonstrates the method effectiveness by achieving the system maximum efficiency. Controllability restrictions preventing the compensation of the most severe parameters variations are highlighted. Associated with the limited voltage producible by conventional full-bridge converters, the latter restrictions are surmounted with success by considering Z-source topologies for the front- and back-end converters.**

***Index Terms*—Active rectification, Bidirectional power flow, Dual active bridge, Wireless power transmission, Z-source converter**

I. Introduction

WIRELESS power transfer (WPT) is a popular and trending topic in the scientific and industrial communities. As a matter of fact, the recent progresses in power electronics have paved the way for the implementation of resonant inductive power transfer to energy-greedy applications, such as electric vehicle (EV) battery charging [1]–[3]. Bringing more convenience and more safety, wireless charging systems for EVs reach currently performances comparable to or even better than classical wire-connected systems [4]. Dealing with high power-levels (from a few kW to tens of kW, typically) requires however to pay a particular attention on the system optimal operation, as each percent of its power efficiency represents a non-negligible amount of power. Based on magnetically coupled resonant circuits, the WPT systems are only effective in a restricted operating range, with respect to the circuit parameters. An adequate command is therefore mandatory for practicable domestic and industrial implementations, which are subject to transmitter-receiver misalignment and/or components deteriorations.

Manuscript received April 19, 2005; revised August 26, 2015.

The operating frequency is obviously a key-parameter for optimizing the performances of a resonant system. Incidentally, the interest of an appropriate frequency variation has been demonstrated [5], [6]. However, variable-frequency control strategies are not addressed in this work as standardization procedures currently tend to impose a fixed frequency for improving WPT systems universality. Moreover, the typical bifurcation phenomenon occurring with resonant coupling threatens the stability and the controllability of the system when the variation in frequency is too important [7]. With a fixed operating frequency, optimal performances can be reached by a suitable sizing of the system load resistance [8]. Based on the latter statement, fixed-frequency control strategies have successfully investigated the modulation of the apparent resistive load thanks to a DC-DC converter interfacing the circuit and the load [9], [10]. Colak *et al.* have further demonstrated the possibility to avoid any additional DC-DC converter while modulating the apparent load by using a semibridgeless active rectifier instead of a conventional diode rectifier for interfacing the secondary circuit with the actual load [11]. Although effective, those strategies aim to solely optimize the active power flow, whereas the reactive power flow - preponderant for a proper resonant operation - is free to vary with the potential deviations in circuit parameters. Therefore, researches have recently investigated the resort to a full-bridge active rectifier for introducing a given phase-shift between the primary and the secondary voltages. Zhao *et al.* have *e.g.* illustrated the feasability of using the non-synchronous rectification for influencing the reactive power flow and further the resonance phenomenon, with nevertheless a simultaneous impact on the optimality of the active power flow [12]. Based on the latter work, an advanced contribution proposed to modulate independently the resistive and the reactive parts of the equivalent load via active rectification for maximizing the efficiency and increasing the deliverable power [13]. To this end, the optimal conditions are obtained numerically via a constrained optimization and an active rectifier followed by an additional DC-DC converter are employed for achieving those conditions, by respectively and independently controlling the secondary voltage phase-shift and regulating its amplitude.

In this paper, we propose an alternative approach to optimize WPT performances via active load modulation, with two main simplification axes. On the one hand, the non-synchronous rectification is performed by controlling the active rectifier using a symmetric voltage cancellation (SVC) command, enabling

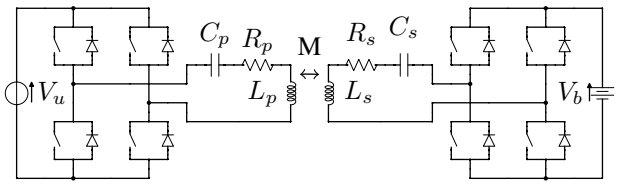

Fig. 1: Proposed resonant WPT topology

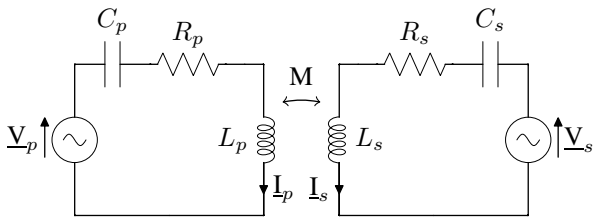

Fig. 2: Equivalent circuit for FHA

the combined control of the amplitude and of the phase of the secondary voltage without any additional DC-DC converter. It results in a topological symmetry which provides power-reversibility capabilities for the resonant WPT system, which is an a farsighted asset since enabling bidirectional powerflows permits to use EVs as storage units for vehicle-to-home (V2H) and vehicle-to-grid (V2G) applications [14]. In contrast, the aforementioned state-of-the-art contributions use asymmetric topologies and are only practicable for a unidirectional power flow. Furthermore, the optimal conditions are here obtained analytically via a simple first harmonic analysis (FHA) of the system equivalent circuit. Both the real and the imaginary parts of the equivalent load impedance are in that way independently controlled for keeping optimal performances and supplying a fixed power despite deviations. Preliminarily presented in [15], this method is subject to restrictions in controllability associated with the limited voltage attainable by conventional converters. For overcoming those restrictions, Z-source converters [16] are investigated in this paper. In the context of WPT, Z-source converters have already been envisioned as front-end converters for improving the systems operation, notably via a power factor correction [17]–[19]. Here, Z-source converters are employed both as an inverter on the source side and as an active rectifier on the load side. To our knowledge, using a Z-source active rectifier has not been proposed yet in the framework of WPT.

The paper is organized as follows. In Section II, the FHA of the proposed WPT topology is proceeded. In Section III, the methodology to achieve these optimal conditions via synchronous rectification is detailed. The proposed approach is validated and analyzed by observing the results obtained under FHA assumptions. Section IV is dedicated to the implementation of the power converters in the time-domain, highlighting restrictions in the controllability which are in turn discussed. For surmounting the latter restrictions, the Z-source concept is outlined. Section V exposes the theoretical bases for Z-source converters and presents the results given by the time-domain implementation of the Z-source converters command following the proposed approach.

II. First Harmonic Analysis of the Proposed Topology

The proposed resonant WPT system topology is presented in Fig. 1. The power transfer is ensured by a near-field magnetic coupling between the primary and secondary windings, with a mutual inductance M. For reducing the volt-ampere rating of both AC circuits, the reactive power flow is cancelled by compensating the series self-inductance of each side L_p and L_s by a series capacitance C_p and C_s, respectively. The system is designed so that the primary and the secondary circuits share a common self-resonant frequency ω_0, *i.e.*

$$\omega_0 = \frac{1}{\sqrt{L_p C_p}} = \frac{1}{\sqrt{L_s C_s}} \tag{1}$$

Operated with an angular frequency ω equal to ω_0, the system displays a theoretical infinite power transfer capability whereas presenting a unitary power efficiency. In practice, these transfer performances are limited by the components parasitic resistances R_p and R_s. Each circuit is connected to a full-bridge converter interfacing the resonant WPT system with the rectified utility voltage V_u on one side and with the battery voltage V_b on the other side. Considering the filtering action of each LC circuit on the converters AC currents, an FHA performed on the equivalent circuit shown in Fig. 2 is sufficient to analyze the system performances and operation. The power converter can be replaced by AC voltage sources as their AC voltage is controllable in module and phase via SVC. For clarity purposes, only the case of a power transfer from the utility to the battery is addressed in the following developments. Given the system topological symmetry, the case of a transfer from the battery to the utility can be treated similarly by interchanging the primary and the secondary roles in the mathematical expressions.

A. Power efficiency and optimal load

For analyzing the power efficiency and given the direction of the useful power, the source $\underline{\mathbf{V}}_s$ is replaced by an equivalent active load $\underline{\mathbf{Z}}_L = R_L + jX_L$. Hence, the active power efficiency can be written as

$$\eta = \frac{R_L I_s^2}{R_p I_p^2 + R_s I_s^2 + R_L I_s^2} \tag{2}$$

where I_p and I_s are the RMS values of the primary and the secondary currents, respectively. The combined primary and secondary circuits resonances are mandatory for maximizing the power efficiency as the cancellation of the reactive power flow ensures a minimal value for I_p and I_s. In this resonant state, the primary and secondary currents can be related as

$$\omega_0 M I_p = (R_s + R_L)\, I_s. \tag{3}$$

Therefore, the power efficiency η becomes

$$\eta = \frac{R_L}{R_p \frac{(R_s+R_L)^2}{\omega_0^2 M^2} + R_s + R_L} \tag{4}$$

which depends on the windings intrinsic parameters such as R_p, R_s or M and on R_L, which can be modulated by controlling adequately the secondary power converter. Hence, the transfer efficiency can be optimized by imposing an optimal load R_L^{opt} so that

$$\frac{\partial \eta}{\partial R_L}\left(R_L^{opt}\right) = 0 \text{ and } \frac{\partial^2 \eta}{\partial R_L^2}\left(R_L^{opt}\right) < 0. \tag{5}$$

After solving Eq. (5), the optimal load is given by

$$R_L^{opt} = R_s\sqrt{1+\frac{\omega_0^2 M^2}{R_p R_s}}. \tag{6}$$

Ensuring $R_L = R_L^{opt}$ guarantees to operate the system at its maximum intrinsically achievable efficiency η_{max}, which is imposed by the design of the LC circuits and given by

$$\eta_{max} = \frac{\omega_0^2 M^2}{R_p R_s\left(1+\sqrt{1+\frac{\omega_0^2 M^2}{R_p R_s}}\right)^2} \tag{7}$$

B. Direct modulation of the load impedance

The combination of an active rectifier with well-designed resonant WPT circuits offers a direct control on the load impedance. By applying the Kirchhoff's voltage law in FHA to the circuit presented in Fig. 2, one has

$$\underline{\mathrm{V}}_p = \underline{\mathrm{Z}}_p\underline{\mathrm{I}}_p + j\omega M\underline{\mathrm{I}}_s \tag{8}$$

$$\underline{\mathrm{V}}_s = \underline{\mathrm{Z}}_s\underline{\mathrm{I}}_s + j\omega M\underline{\mathrm{I}}_p \tag{9}$$

with j the imaginary unit (so that $j=\sqrt{-1}$) and with

$$\underline{\mathrm{Z}}_p = R_p + j\omega L_p + 1/j\omega C_p \tag{10}$$

$$\underline{\mathrm{Z}}_s = R_s + j\omega L_s + 1/j\omega C_s. \tag{11}$$

Solving (8) and (9), the expressions of the currents are

$$\underline{\mathrm{I}}_p = \frac{\underline{\mathrm{Z}}_s\underline{\mathrm{V}}_p - j\omega M\underline{\mathrm{V}}_s}{\underline{\mathrm{Z}}_p\underline{\mathrm{Z}}_s + \omega^2 M^2} \tag{12}$$

$$\underline{\mathrm{I}}_s = \frac{\underline{\mathrm{Z}}_p\underline{\mathrm{V}}_s - j\omega M\underline{\mathrm{V}}_p}{\underline{\mathrm{Z}}_p\underline{\mathrm{Z}}_s + \omega^2 M^2}. \tag{13}$$

By observing Eq. (13), one can observe that the secondary current $\underline{\mathrm{I}}_s$ is quasi-independent from the secondary voltage $\underline{\mathrm{V}}_s$ at the resonant frequency ω_0, as $\underline{\mathrm{Z}}_p = R_p \approx 0$ at ω_0 for properly designed coils. Therefore, modifying $\underline{\mathrm{V}}_s$ amounts to modulate directly the equivalent load impedance $\underline{\mathrm{Z}}_L$ as seen from the secondary terminals, defined as

$$\underline{\mathrm{Z}}_L = -\underline{\mathrm{V}}_s/\underline{\mathrm{I}}_s. \tag{14}$$

As a consequence, the real and imaginary parts of the equivalent load impedance can be adjusted independently by controlling the secondary voltage $\underline{\mathrm{V}}_s$ in module and in phase. On the other hand, the transferred power can be regulated by controlling the primary voltage $\underline{\mathrm{V}}_p$, which determines $\underline{\mathrm{I}}_s$.

III. Methodology

Assuming that the system is operated at the primary self-resonant frequency (*i.e.*, that $\omega = 1/\sqrt{L_pC_p}$), the direct modulation of the load impedance is practicable as described above. The control strategy consists in simultaneously maximizing the power efficiency and setting the output power.

A. Maximization of the power efficiency

According to the developments above, the system achieves its maximum intrinsic power efficiency η_{max} when the secondary total reactance is null while the equivalent load resistance seen from its terminals is R_L^{opt}. The equivalent load impedance $\underline{\mathrm{Z}}_L$ must be equal to

$$\underline{\mathrm{Z}}_L = R_L^{opt} + jX_L^{opt} \tag{15}$$

where X_L^{opt} ensures the cancellation of the reactive power in the secondary circuit in the case of a mistuned secondary circuit (*i.e.*, when $L_pC_p \neq L_sC_s$), with

$$X_L^{opt} = \frac{1}{\omega C_s} - \omega L_s. \tag{16}$$

One can note that X_L^{opt} is null when the secondary is correctly tuned (*i.e.*, when $\omega = 1/\sqrt{L_pC_p} = 1/\sqrt{L_sC_s}$). The secondary voltage can be shifted in phase for emulating a reactive function thanks to the active rectification, which is not practicable with classical topologies. Mathematically, the condition for achieving η_{max} is written as

$$\underline{\mathrm{V}}_s = -\underline{\mathrm{Z}}_L^{opt}\underline{\mathrm{I}}_s. \tag{17}$$

By eliminating the current (13) in (17), the condition becomes

$$j\omega\underline{\mathrm{Z}}_L^{opt}M\underline{\mathrm{V}}_p + \left(\underline{\mathrm{Z}}_p\underline{\mathrm{Z}}_z + \omega^2M^2 + \underline{\mathrm{Z}}_L^{opt}\underline{\mathrm{Z}}_p\right) = 0 \tag{18}$$

which is a first equation linking the complex values $\underline{\mathrm{V}}_p$ and $\underline{\mathrm{V}}_s$. One can observe that the condition (18) accounts for the parasitic resistances in the relation between $\underline{\mathrm{V}}_s$ and $\underline{\mathrm{I}}_s$.

B. Setting the output power

Achieving a reference active power P_{ref} to the load is accomplished by setting adequately the module of the secondary current. Indeed, assuming that condition (18) is achieved, the real part of the load is equal to R_L^{opt} so that a power P_{ref} is transmitted to the load when

$$I_s = \sqrt{P_{ref}/R_L^{opt}} \tag{19}$$

Considering Eq. (13) and reminding that $\underline{\mathrm{Z}}_p \approx 0$, the current $\underline{\mathrm{I}}_s$ lags the voltage $\underline{\mathrm{V}}_p$ (taken as the phase reference) by $\pi/2$ radians, so that the complex condition ensuring the transfer of a power P_{ref} is

$$\underline{\mathrm{I}}_s = \sqrt{P_{ref}/R_L^{opt}}e^{-j\frac{\pi}{2}}. \tag{20}$$

From (13) and (20), the condition becomes

$$\frac{\underline{\mathrm{Z}}_p\underline{\mathrm{V}}_s - j\omega M\underline{\mathrm{V}}_p}{\underline{\mathrm{Z}}_p\underline{\mathrm{Z}}_s + \omega^2 M^2} = \sqrt{P_{ref}/R_L^{opt}}e^{-j\frac{\pi}{2}} \tag{21}$$

which is a second equation linking the values $\underline{\mathrm{V}}_p$ and $\underline{\mathrm{V}}_s$. Finally, the desired setting point is reached by imposing the voltages $\underline{\mathrm{V}}_p$ and $\underline{\mathrm{V}}_s$ solving simultaneously the equations (18) and (21).

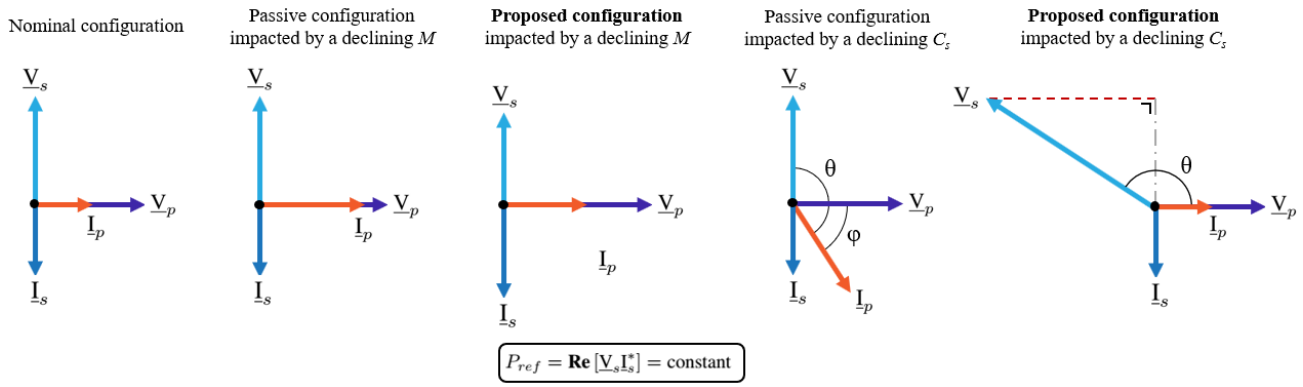

Fig. 3: Voltages and currents phasors relative to a decrease of M and to a decrease of C_s

C. Illustration

The main principle of the methodology is illustrated on a test-case via Matlab simulations. The nominal circuit parameters are gathered in Table I (with $f = \omega/2\pi$ the operating frequency). The system is expected to supply a reference output power $P_{ref} = 3.7$ kW to the load. For comparison purposes, the optimal performances of the proposed system are contrasted with the performances of a *passive* system, which is optimally designed for the nominal value of the circuit parameters only. Two illustrations examples are considered. Firstly, the decrease of the mutual inductance M is addressed as the most important case because very likely and frequently occurring during the system operation (due to windings misalignment). Impacting R_L^{opt}, such a case challenges the active power modulation of the proposed method. Secondly, the decrease of C_s (*e.g.*, due to the deterioration of the related capacitor) is tackled. Rarely happening during the system operation but impacting X_L^{opt}, this case permits to validate the reactive power modulation abilities of the proposed system.

f	$R_p = R_s$	$L_p = L_s$	$C_p = C_s$	M
85 kHz	0.1 Ω	70 μH	50 nF	8 μH

TABLE I: Nominal parameters of the test-case circuit

Observing the voltages and currents phasors (see Fig. 3) permits an intuitive understanding of the action of the proposed method. For a passive configuration, a decline in M increases significantly the primary current $\underline{I}_p$ since the system has to achieve a constant output power despite harsher coupling conditions. The power efficiency is deteriorated due to increased Joule losses (see the left graph on Fig. 4). Facing up those conditions, the proposed method takes an action on the voltages $\underline{V}_p$ and $\underline{V}_s$ for a fairer repartition of the losses in the circuit, by increasing and decreasing the currents $\underline{I}_s$ and $\underline{I}_p$, respectively. Despite an M decrease, the proposed configuration achieves hence the maximum efficiency. The latter is therefore optimal, but inevitably lower than the nominal efficiency due to the detrimental effect of a diminution of M on the maximum intrinsically achievable efficiency (as described by Eq. (7)). Also, the volt-ampere (VA) ratings are smaller on both sides. For passive configurations, a lowering of C_s raises drastically the primary current $\underline{I}_p$ since the system has to

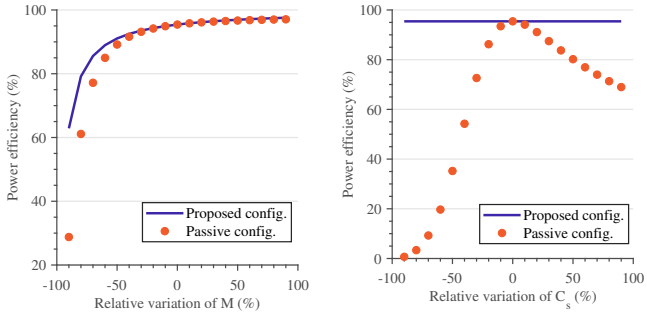

Fig. 4: Evolution of the different configurations power efficiency for variations of M (left) and of C_s (right)

achieve a constant output power despite an increasing phase shift φ between the primary current $\underline{I}_p$ and voltage $\underline{V}_p$. As a consequence, the system efficiency drops significantly due to Joule losses (see the right graph on Fig. 4). By performing an active rectification, the proposed method shifts the secondary voltage $\underline{V}_s$ which sweeps the solidary current $\underline{I}_p$ away (as θ is constant for a given variation of C_s) until its alignment with the voltage $\underline{V}_p$. The mistuning penalty is displaced from the primary current $\underline{I}_p$ to the secondary voltage $\underline{V}_s$, with a consequential rise of the secondary VA rating. However, both currents $\underline{I}_p$ and $\underline{I}_s$ are back in their nominal position so that the deleterious impact of a C_s variation on the system efficiency is fully compensated. One can notice that a spontaneous rise of C_s is unlikely in practice. However, illustrating such a case in Fig. 4 permits to virtually demonstrate the intrinsic compensation capabilities of the system. As a matter of fact, these two examples can be extended to deviations of any other circuit parameter. Holistically, variations of R_p and R_s have similar effects as M variations, and can thus be compensated analogously. The same philosophy prevails between L_s variations and C_s variations. Finally, variations of L_p and/or C_p produce a deviation of the working angular frequency ω which can be compensated as combined deviations of M and C_s.

IV. Voltage-Source Converters Implementation

So far, the methodology has been developed and illustrated considering ideal and sinusoidal voltage sources. In this section, the actual voltage-source converters (see Fig. 1) and the related pulse-width modulation (PWM) commands are practically implemented in a realistic time-domain model

This article has been accepted for publication in a future issue of this journal, but has not been fully edited. Content may change prior to final publication. Citation information: DOI 10.1109/TIA.2020.2966161, IEEE Transactions on Industry Applications

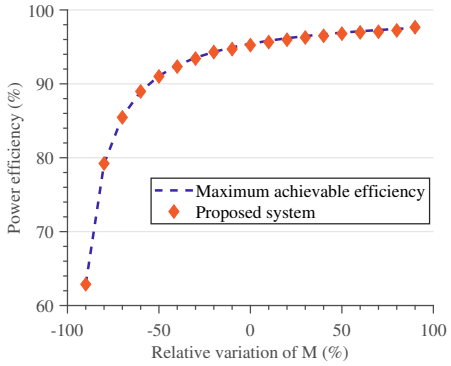

Fig. 5: Simulated measurement of the power efficiency for a deviation of M impacting the proposed system

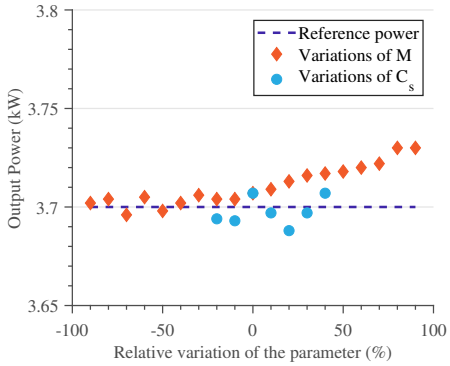

Fig. 7: Simulated measurement of the output power for deviations of M and C_s impacting the proposed system

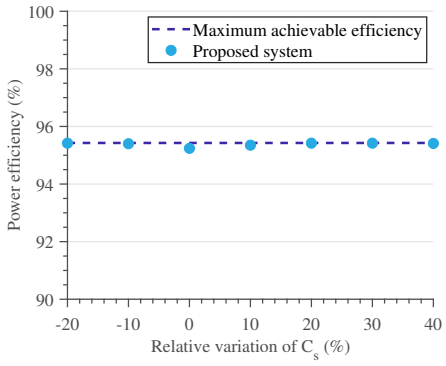

Fig. 6: Simulated measurement of the power efficiency for a deviation of C_s impacting the proposed system

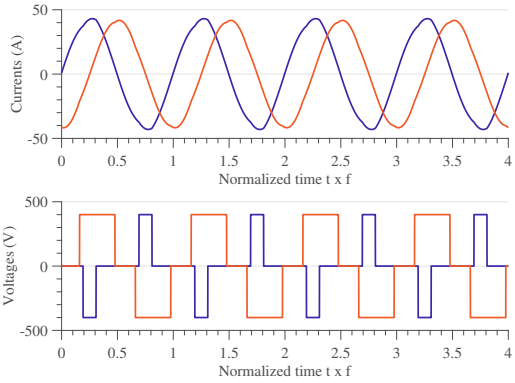

Fig. 8: Simulated primary (blue) and secondary (orange) waveforms from the proposed system for a -20 % C_s deviation

running under the PSIM software. Consistently, the WPT test-case described in Table I is anew considered. The time-step is fixed to 10^{-7} second. MOSFETs have been selected as actual switching devices and the voltages V_u and V_b are both fixed to 400 V in compliance with utility and EV batteries common voltage levels. The converters are controlled following an SVC scheme and produce voltages presenting fundamentals which satisfy equations (18) and (21).

A. Time-domain simulation results

Mutual inductance M and secondary capacitance C_s variations are applied to the system. This time-domain implementation aims to verify the relevance of the FHA-based methodology, despite the enriched harmonic content of the actual voltage waves. The corresponding time-domain results are compared to target operating points computed in the frequency-domain (see Fig. 5 to 7). One can ascertain that the proposed methodology leads to an optimal operation of the system, despite parameters deviations. Notably, the aforementioned LC-circuits filtering effect is demonstrated by the proximity of time-domain and frequency-domain results and is qualitatively appreciable by observing currents waveforms on Fig. 8. The latter findings legitimate the FHA-based methodology despite non-sinusoidal voltage waveforms. The system performs with a clear effectiveness when facing the key-case of a coupling variation. However, the applicability of the proposed approach is restricted since the simulated system is not able to compensate C_s variations greater than -20 % or +40 %. This restriction correlates with the limited voltage range of the converters, as discussed hereafter.

B. Highlight on the controllability restrictions

Among the different non-idealities of conventional voltage-source converters, the limitation in producible voltage is the cause of the aforementioned controllability restrictions. As a matter of fact, the amplitude of the voltage on the converter AC-side is limited by the DC-side voltage source. Implementing an SVC command, the RMS value $V_{AC}^{(1)}$ of the fundamental of the AC voltage produced by a converter is

$$V_{AC}^{(1)} = \frac{2\sqrt{2}}{\pi} V_{DC} \sin\left(\beta/2\right) \tag{22}$$

where V_{DC} is the voltage on the DC-side of the converter (which is *a priori* fixed by the related source) and β is the SVC conduction angle. As a consequence, the maximal practicable AC voltage module is $\frac{2\sqrt{2}}{\pi} V_{DC}$, so that some solutions of equations (18) and (21) - requiring primary and/or secondary RMS voltage higher than $\frac{2\sqrt{2}}{\pi} V_u$ and $\frac{2\sqrt{2}}{\pi} V_b$, respectively - are not achievable in practice. Yet, in the aforementioned case of a variation of C_s, the proposed method tends to largely increase the module of the secondary voltage for shifting it

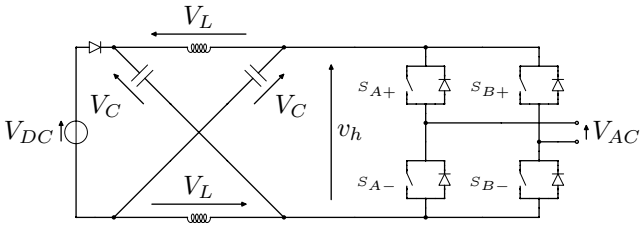

Fig. 9: Z-source converter

while keeping constant the output power, as shown in Fig. 3 and as previously explained. Compensations for severe C_s deviations are henceforth not reachable with the secondary converter, since the latter is not able to achieve a sufficient voltage. Although not addressed with the featured simulations, other situations can lead to similar issues and can also be pertaining to the primary converter (*e.g*, in the case of the setting of a higher reference power P_{ref}). Reversible boost converters could be a solution to this issue complying with the power bidirectionality requirements. Nevertheless, this choice would lead to the inclusion of additional converters, which is a practice that we criticized in our state-of-the-art analyze. Hence, a transition to Z-source topologies is an elegant and a consistent way to extend the method applicability without requiring extra power converters.

V. Extension of the Method Applicability using the Z-source Topology

A Z-source converter [16] is a unique structure combining a specific impedance network with a conventional converter adequately commanded (see Fig. 9). Developed for notably overcoming the drawbacks of voltage-source converters, the Z-source topology enables the generation of AC voltages with any value between zero and infinity theoretically. The development leading to this particular feature is detailed hereafter.

A. Impedance network and shoot-through state

The Z-source impendance network consists in a two-port network including two inductors interconnected with two cross-shaped capacitors. Presenting current limitation properties, this specific topology tolerates the shorting of the converter legs (*i.e.*, the closing of both switching devices equipping a same leg) which is forbidden with a conventional converter for ensuring its integrity. In addition to the conventional active (*i.e.*, when the converter produces a non-zero voltage) and freewheeling states, the Z-source converter disposes of an extra state corresponding to the shorting of one of its legs, called the *shoot-through* state. An additional diode protects the DC voltage source from hazardous current during shoot-through states. Combined with the reactive nature of the Z-source impedance network, the shoot-through state grants an additional degree of freedom in the converter command for achieving any output voltage.

B. Circuit analysis

For simplicity purposes, we assume that both inductors and both capacitors have respectively the same inductance and the same capacitance, making the Z-source network symmetric. Moreover, the common inductance and capacitance are supposed to be high enough for considering the inductors equal currents I_L and the capacitors equal voltages V_C constant. Focusing on the elementary analysis of the Z-source converter operation, the active (A) and freewheeling (FW) states can be treated similarly. During these states (prevailing respectively for total portions D_A and D_{FW} of the period T), the voltages in the circuit are

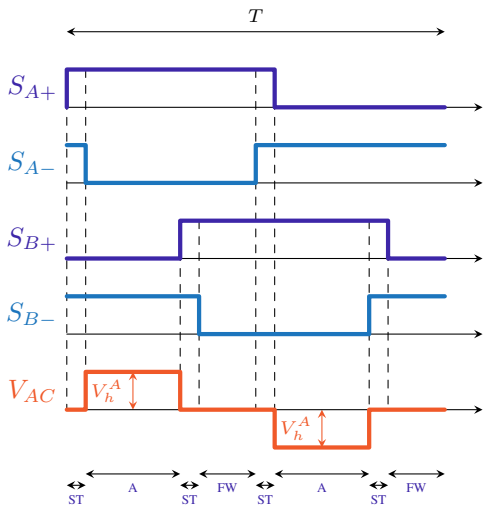

Fig. 10: Proposed Z-source converters control scheme

$$v_L = V_{DC} - V_C \qquad v_h = 2V_C - V_{DC} \tag{23}$$

During the shoot-through (ST) state (prevailing for a total portion D_{ST} of the period T), the voltages in the circuit are

$$v_L = V_C \qquad v_h = 0 \tag{24}$$

In steady state, the system is characterized by the absence of net energy storage in the reactive elements on a working period. Notably, the mean inductors voltage $\bar{v}_L$ must be null. One has

$$\bar{v}_L = (D_A + D_{FW})(V_{DC} - V_C) + D_{ST}V_C = 0 \tag{25}$$

leading to the value of the capacitors voltage V_C

$$V_C = \frac{1 - D_{ST}}{1 - 2D_{ST}} V_{DC}. \tag{26}$$

When the converter is in the active state, the voltage on the DC-side of the full-bridge V_h^A is theoretically constant and equal to

$$V_h^A = 2V_C - V_{DC} = \frac{1}{1 - 2D_{ST}} V_{DC}. \tag{27}$$

During the active states, the Z-source converter can therefore produce a DC voltage V_h^A ranging from V_{DC} to infinity by introducing shoot-through states with $0 \leq D_{ST} < 0.5$. As a consequence, the module of the fundamental AC voltage produced by the converter can be worth any value between zero and infinity. Here, a variant of an SVC command integrating shoot-through states while ensuring a uniform repartition of the constraint on the switches (in terms of conduction time

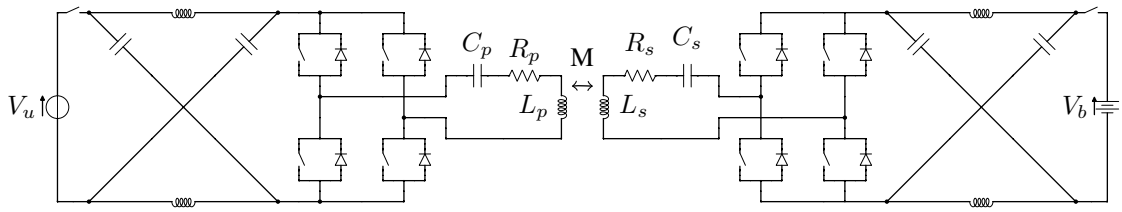

Fig. 11: Improved proposition of resonant WPT topology

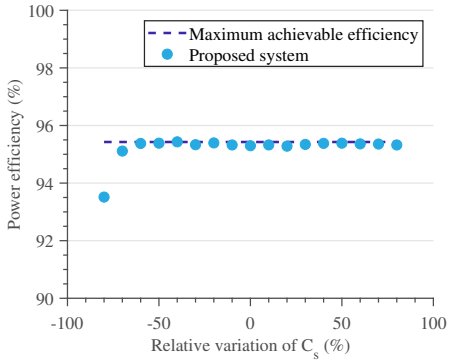

Fig. 12: Simulated measurement of the power efficiency for a deviation of C_s impacting the improved system

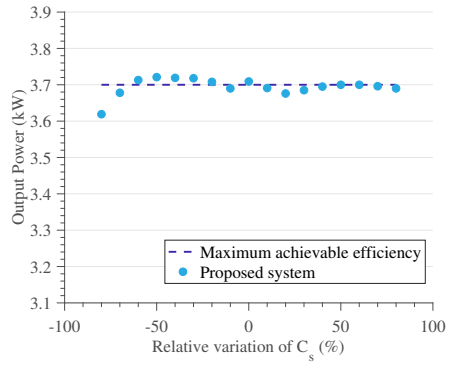

Fig. 13: Simulated measurement of the output power for a deviation of C_s impacting the improved system

and shoot-throughs) is proposed. Referring to the notations on Fig. 9, the corresponding gate signals of the switches and the resulting AC voltage are represented on Fig. 10. Under those conditions, the RMS value of the fundamental of the Z-source converter AC voltage is given by

$$V_{AC}^{(1)} = \frac{2\sqrt{2}}{\pi} \frac{V_{DC}}{1-2D_{ST}} \sin\left[\frac{(1-D_{ST}-D_{FW})\,\pi}{2}\right] \quad (28)$$

which can take any value between zero and infinity by an adequate choice of D_{ST} and D_{FW}. Therefore, the restrictions experienced in Section IV are overcome without any additional converter. Finally, one can notice that the present development does not rely on the current direction so that the Z-source topology complies with our reversibility requirements by replacing the DC-source diode by a bidirectional switch.

C. Implementation and discussions

Z-source impedance networks are introduced on both primary side and secondary side converters (see Fig. 11 for the resulting circuit). The problematical case of a C_s variation is anew considered with this improved circuit. The time-domain simulation of the latter is carried out on the PSIM software and the associated results are presented on Fig. 12 and 13. One can observe the positive impact of the Z-source converters on the extent of the proposed method. Nonetheless, the two most severe decreases in C_s deviate slightly from the expected set points. Actually, the required fundamental RMS value for the secondary voltage in these cases is significantly higher. For increasing the boost-effect, the command tends to enlarge the duration of shoot-through states during which the secondary LC-oscillator current is free to vary (see Fig. 14). The latter current is therefore more distorted (with total harmonic distortion touching 88.33 % in the most severe case) and the assumptions of the proposed FHA-based approach are consequently less respected. A potential solution to this issue might be a supplemented control scheme with notably a higher switching frequency (which is though difficult to envision regarding the current state-of-the-art performances of switching devices in the targeted power range). Besides this operational concern, the Z-source converter presents an intrinsic practical issue since it requires to raise the voltage rating for the circuit components. Indeed, from the AC-side of the converter, an increase of D_{ST} widens the zero-state in the AC voltage waveform, leading to a significant decrease of the RMS value of the related fundamental as expressed mathematically by the sine argument in Eq. (28). For achieving a high voltage despite the rise of D_{ST}, the command scales up therefore the voltage V_h^A (which has to be supported by the switches). This is clearly observable in Fig. 15 where the RMS voltage required by the proposed approach is contrasted with the related DC-side voltage using a Z-source converter. For comparison purposes, the related DC-side voltage using an additional conventional boost converter in cascade with the active rectifier is also represented.

VI. Conclusion

In this paper, a method employing an active rectification for the optimal control of a bidirectional resonant WPT system is proposed. Benefiting from a resonant dual active bridge topology, the real and especially the imaginary parts of the equivalent load impedance can be modulated simultaneously and independently by controlling adequately the active rectifier switches. The command methodology development is based on a simple FHA (thanks to the important filtering effect provided by the resonant system) and ensures that the system delivers the required output power at its maximum achievable efficiency, despite sensible deviations in the circuit parameters. Using FHA, the effectiveness of the method has

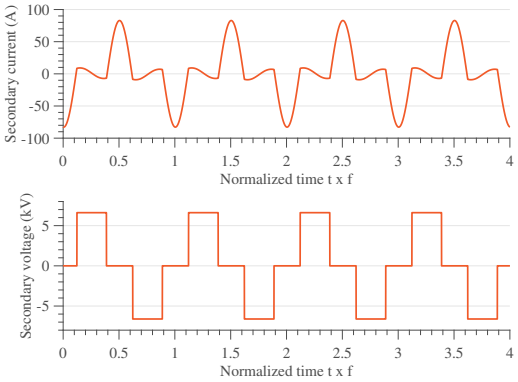

Fig. 14: Secondary current (up) and voltage (down) for a C_s deviation of -80 % impacting the improved system

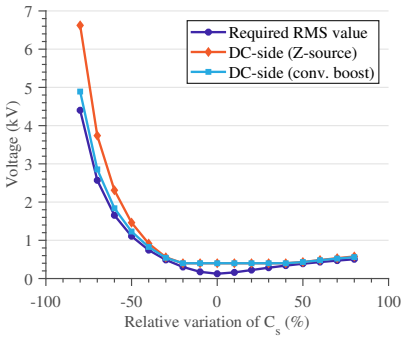

Fig. 15: Required DC voltage for ensuring a given voltage RMS value (Z-source and conventional boost converters configurations)

been shown and discussed against variations in the windings mutual inductance M (impacting the active power flow) and in the secondary capacitance C_s (impacting both the active and the reactive power flows). By extension, we acknowledged its effectiveness against any variation in any parameter in the circuit. The proposed converters topology and command have been implemented and simulated using a time-domain model, demonstrating the proposed method validity despite the non-compliance with the FHA assumptions (notably despite more realistic non-sinusoidal voltage waveforms).

Nevertheless, some controllability restrictions emerged with the time-domain implementation of the proposed methodology. Hence, the limitation in voltage producible by the converters reduces the compensation capabilities of the system, unable to produce a sufficient voltage for reaching the targeted optimal operating point in case of severe circuit parameters deviations. For surmounting these restrictions without requiring any additional converter, Z-source converters have been used. As exposed via a brief theoretical reminder, the Z-source topology allows the converters to produce any voltage between zero and infinity, notionally. The time-domain implementation of the improved topology (including Z-source instead of conventional converters) has demonstrated the removal of the aforementioned restrictions. Implemented on such a topology, the proposed method is capable to counter efficiently the most severe deviations in parameters as significant as the secondary resonator capacitance C_s. The establishment of a closed-loop control scheme and the constitution of a reduced power experimental prototype are envisioned as further work.

REFERENCES

[1] G. A. Covic and J. T. Boys, "Modern trends in inductive power transfer for transportation applications," *IEEE Journal of Emerging and Selected Topics in Power Electronics*, vol. 1, no. 1, pp. 28–41, March 2013.

[2] S. Li and C. C. Mi, "Wireless power transfer for electric vehicle applications," *IEEE Journal of Emerging and Selected Topics in Power Electronics*, vol. 3, no. 1, pp. 4–17, March 2015.

[3] K. A. Kalwar, M. Aamir, and S. Mekhilef, "Inductively coupled power transfer (icpt) for electric vehicle charging a review," *Renewable and Sustainable Energy Reviews*, vol. 47, pp. 462 – 475, 2015.

[4] R. Bosshard and J. W. Kolar, "Inductive power transfer for electric vehicle charging: Technical challenges and tradeoffs," *IEEE Power Electronics Magazine*, vol. 3, no. 3, pp. 22–30, Sept 2016.

[5] A. P. Sample, D. T. Meyer, and J. R. Smith, "Analysis, experimental results, and range adaptation of magnetically coupled resonators for wireless power transfer," *IEEE Transactions on Industrial Electronics*, vol. 58, no. 2, pp. 544–554, Feb 2011.

[6] D. Patil, M. Sirico, L. Gu, and B. Fahimi, "Maximum efficiency tracking in wireless power transfer for battery charger: Phase shift and frequency control," in *2016 IEEE Energy Conversion Congress and Exposition (ECCE)*, Sept 2016, pp. 1–8.

[7] C.-S. Wang, O. H. Stielau, and G. A. Covic, "Design considerations for a contactless electric vehicle battery charger," *IEEE Transactions on Industrial Electronics*, vol. 52, no. 5, pp. 1308–1314, Oct 2005.

[8] H. Li, X. Yang, K. Wang, and X. Dong, "Study on efficiency maximization design principles for wireless power transfer system using magnetic resonant coupling," in *2013 IEEE ECCE Asia Downunder*, June 2013, pp. 888–892.

[9] H. Li, J. Li, K. Wang, W. Chen, and X. Yang, "A maximum efficiency point tracking control scheme for wireless power transfer systems using magnetic resonant coupling," *IEEE Transactions on Power Electronics*, vol. 30, no. 7, pp. 3998–4008, July 2015.

[10] W. X. Zhong and S. Y. R. Hui, "Maximum energy efficiency tracking for wireless power transfer systems," *IEEE Transactions on Power Electronics*, vol. 30, no. 7, pp. 4025–4034, July 2015.

[11] K. Colak, E. Asa, M. Bojarski, D. Czarkowski, and O. C. Onar, "A novel phase-shift control of semibridgeless active rectifier for wireless power transfer," *IEEE Transactions on Power Electronics*, vol. 30, no. 11, pp. 6288–6297, Nov 2015.

[12] C. Zhao, Z. Wang, J. Du, J. Wu, S. Zong, and X. He, "Active resonance wireless power transfer system using phase shift control strategy," in *2014 IEEE Applied Power Electronics Conference and Exposition - APEC 2014*, March 2014, pp. 1336–1341.

[13] A. Berger, M. Agostinelli, S. Vesti, J. A. Oliver, J. A. Cobos, and M. Huemer, "A wireless charging system applying phase-shift and amplitude control to maximize efficiency and extractable power," *IEEE Transactions on Power Electronics*, vol. 30, no. 11, pp. 6338–6348, Nov 2015.

[14] U. K. Madawala and D. J. Thrimawithana, "A bidirectional inductive power interface for electric vehicles in v2g systems," *IEEE Transactions on Industrial Electronics*, vol. 58, no. 10, pp. 4789–4796, Oct 2011.

[15] A. Desmoort, O. Deblecker, and Z. De Grve, "Active rectification for the optimal control of bidirectional resonant wireless power transfer," in *2018 International Symposium on Power Electronics, Electrical Drives, Automation and Motion (SPEEDAM)*, June 2018, pp. 756–761.

[16] F. Z. Peng, "Z-source inverter," in *Conference Record of the 2002 IEEE Industry Applications Conference. 37th IAS Annual Meeting (Cat. No.02CH37344)*, vol. 2, Oct 2002, pp. 775–781 vol.2.

[17] N. S. Gonzlez-Santini, H. Zeng, Y. Yu, and F. Z. Peng, "Z-source resonant converter with power factor correction for wireless power transfer applications," *IEEE Transactions on Power Electronics*, vol. 31, no. 11, pp. 7691–7700, Nov 2016.

[18] W. Tianfeng, L. Xin, T. Houjun, D. Yayun, and Y. Xijun, "Modeling and advanced control of wireless power transfer system with z-source inverter," in *2016 IEEE 2nd Annual Southern Power Electronics Conference (SPEC)*, Dec 2016, pp. 1–6.

[19] H. Zeng, X. Wang, and F. Z. Peng, "High power density z-source resonant wireless charger with line frequency sinusoidal charging," *IEEE Transactions on Power Electronics*, vol. 33, no. 12, pp. 10 148–10 156, Dec 2018.